An NSGA-II Optimized Manifold Microchannel Heat Sink With Better Heat Dissipation and Superior Thermal Uniformity for SiC Power Modules

Chunyang Man, *Student Member, IEEE*, Zhiqiang Wang, *Senior Member, IEEE*, Yu Liao, *Student Member, IEEE*, Xiaojie Shi, *Senior Member, IEEE*, Guoqing Xin, *Member, IEEE*, Yonggang Yao, *Member, IEEE*, and Run Hu, *Member, IEEE*

***Abstract*—Silicon carbide (SiC) power modules are a favorable option for renewable energy and electric vehicles, thanks to the superior performance of SiC bare dies. However, thermal management issues, such as high heat flux and poor thermal uniformity, have been identified as major constraints on the performance improvement of SiC power modules in practical applications. To address these challenges, this article proposes an automated optimization methodology based on the nondominated sorting genetic algorithm with an elite strategy and finite-element analysis for the manifold microchannel (MMC) heat sink. The optimized MMC heat sink is fabricated on a three-phase SiC power module for a thermal performance evaluation through a dedicated thermal test platform. Experimental results show that the optimized MMC heat sink improves the thermal uniformity by 55.6%, reduces the maximum junction-to-fluid thermal resistance of the SiC power module by 9.2% in comparison to the traditional pin-fin heat sink, and simultaneously decreases the total weight of the SiC power module with a cold plate by 8.7%.**

***Index Terms*—Manifold microchannel (MMC), nondominated sorting genetic algorithm with an elite strategy (NSGA-II), silicon carbide (SiC) power modules, thermal management, thermal resistance, thermal uniformity.**

I. Introduction

As energy and environmental issues take center stage, the development of renewable energy and the widespread adoption of electric vehicles have become crucial focal points for many countries. Power electronic converters, as a vital component of electric vehicle power transmission, are garnering increased importance. Ensuring the reliability of these converters is essential for the safety of electrified transportation vehicles. Moreover, due to space and payload limitations, power electronic converters in electrified vehicles are moving toward miniaturization, lightweight design, and high power density [1], [2].

In recent years, silicon carbide (SiC) devices have been demonstrated to be more suitable than silicon (Si) power devices for high-power-density power electronic converters due to their superior electrical and thermal performance [3]. However, as the dimensions of SiC devices diminish, there is a substantial increase in heat flux, reaching levels of a few kW/cm^2 in some SiC power modules [4]. Such high heat flux can severely impact the reliability and longevity of SiC power modules [5]. As shown in Fig. 1(a), statistics indicate that failures induced by temperature factors account for up to 55% of power semiconductor failures. Moreover, within the normal operating temperature range, for every 10 °C increase in junction temperature, the failure rate approximately doubles (known as the 10 °C rule) [6]. Fig. 1(b) shows the weight distribution of major components in the electric drive inverter of the Nissan LEAF, where the thermal management system accounts for the largest share (37%), followed by the power module (23%) [7]. Therefore, developing an efficient and lightweight thermal management system for power

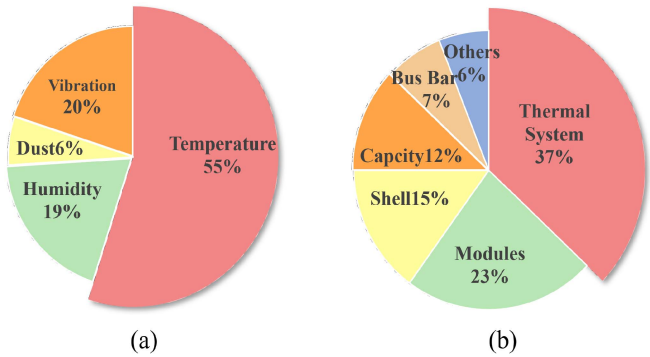

Fig. 1. (a) Power semiconductor failures factors. (b) Weight distribution of major components in the electric drive inverter.

Received 4 November 2024; revised 17 January 2025; accepted 8 March 2025. Date of publication 12 March 2025; date of current version 14 April 2025. This work was supported in part by the National Natural Science Foundation of China under Grant 52277179 and in part by the Science and Technology Project of China Southern Power Grid Corporation under Grant GDKJXM20222074. Recommended for publication by Associate Editor K. Ma. *(Corresponding author: Zhiqiang Wang.)*

Chunyang Man, Zhiqiang Wang, Yu Liao, Xiaojie Shi, and Guoqing Xin are with the School of Electrical and Electronic Engineering, Huazhong University of Science and Technology, Wuhan 430074, China (e-mail: mcy@hust.edu.cn; zhiqiangwang@hust.edu.cn; liaoyu@gddky.csg.cn; xiaojie_shi@hust.edu.cn; guoqingxin@hust.edu.cn).

Run Hu is with the School of Energy and Power Engineering, Huazhong University of Science and Technology, Wuhan 430074, China (e-mail: hurun@hust.edu.cn).

Yonggang Yao is with the School of Materials Science and Engineering, Huazhong University of Science and Technology, Wuhan 430074, China (e-mail: yaoyg@hust.edu.cn).

Color versions of one or more figures in this article are available at https://doi.org/10.1109/TPEL.2025.3550549.

Digital Object Identifier 10.1109/TPEL.2025.3550549

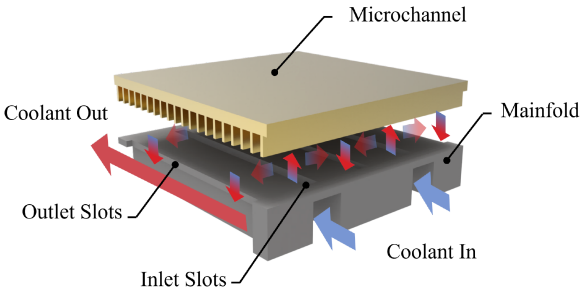

Fig. 2. Physical structure of the MMC.

modules is essential to enhance the overall application of power electronic converters in electric vehicles.

Several cooling methods have been proposed for managing the heat generated by power modules. These methods fall into three main categories: air cooling, liquid cooling, and phase-change cooling [8], [9]. Traditional air cooling is not sufficient for high heat flux, leading to the development of new liquid cooling solutions, such as microchannels [10], jet impingement [11], phase-change cooling [12], and immersion cooling [13].

However, microchannels and jet impingement can result in a significant drop in coolant inlet pressure and require higher pumping power. In addition, phase-change cooling and immersion cooling have complex structures, making it challenging to achieve a compact system, and their reliability is also a concern.

Numerous studies have also been conducted on optimizing heat sink designs. For instance, topology optimization has been applied to the direct water-cooled microelectronic heat sink, achieving a balance between thermal resistance and pressure drop [14]. In addition, parametric scans and comparative analyses have been employed to optimize the liquid-cooled heat sink for electric vehicle inverter modules, resulting in a novel configuration that achieved a high power density of 9.677 kW/kg [15]. Furthermore, genetic algorithms have been used to autonomously optimize an air-cooled inverter, achieving a power density of 75 W/in^3 with a junction temperature of 103 °C [16]. These methods represent common approaches in the field of thermal management research.

In recent years, a promising structure known as manifold microchannels (MMCs) has been extensively investigated for high-heat-flux applications in power electronics [17]. Compared to the aforementioned cooling techniques, the MMC can obtain better heat dissipation performance within a compact volume while maintaining a low pressure drop at the inlet [18]. Some experiments have demonstrated the feasibility of its excellent thermal performance in practical applications [19], [20]. Fig. 2 shows the typical physical structure and water flow direction of the MMC. Although the MMC has many advantages, it also has the following limitations.

1) Compared to the conventional heat sink, the MMC features a more complex structure that requires the integration of specialized manifolds.
2) The small size of the fins necessitates high-precision manufacturing, which increases costs. Moreover, the narrow channels demand high coolant purity to avoid clogging.
3) Like the traditional heat sink, the MMC can exhibit temperature gradients when applied to power module cooling, resulting in thermal nonuniformity issues.

MMCs have been extensively studied, including numerical thermal simulations [21], structural optimization [22], [23], and uniform flow distribution [24]. These studies focused on enhancing the overall cooling capacity to achieve uniform heat flux removal across the entire substrate.

However, similar to traditional cooling methods, the MMC heat sink can also induce a temperature gradient along the flow direction of the coolant, leading to thermal nonuniformity across the power module [25], [26]. Therefore, corresponding thermal management strategies should be developed based on the thermal nonuniformity of the power modules to improve their thermal uniformity metrics of the power modules.

This article improves the thermal nonuniformity and thermal resistance of the SiC power modules by designing a new MMC heat sink using the nondominated sorting genetic algorithm with an elite strategy (NSGA-II) [27] and finite-element analysis (FEA). The rest of this article is organized as follows. In Section II, we analyze the causes of thermal uniformity issues in commercial SiC power modules and propose an automated optimized methodology for the heat sink optimization of power modules using the NSGA-II and FEA. In Section III, the proposed methodology is implemented for a custom-designed SiC power module, leading to the development of a new MMC heat sink. And its thermal efficacy is validated through simulation. Experimental evaluation has been conducted in Section IV. Finally, Section V concludes this article.

II. Proposed Design Methodology

A. Thermal Uniformity Issue of the Commercial Power Module

To investigate the thermal management issues encountered in the practical application of SiC power modules. This section presents a case study focusing on the Onsemi 900-V/620-A single-sided direct liquid-cooled SiC power module. Its structure is shown in Fig. 3. Thermal simulation analysis is carried out using the FEA simulation software COMSOL. The power module's phase leg is constructed with a parallel design that incorporates eight SiC MOSFET dies. The baseplate is directly integrated with a traditional pin-fin heat sink structure, which has a height of 5.8 mm. Table I presents an exhaustive inventory of the thermal parameters pertaining to the diverse packaging materials and cooling fluids employed in the simulation. The pin-fin structure is composed of copper, while the cold plate is made of an aluminum alloy. The chosen cooling fluid is a solution containing 50% volume fraction of ethylene glycol with a dynamic viscosity of 0.406 mPa·s.

In the FEA simulation, several assumptions are made to alleviate the computational burden of the model.

1) The dissipated heat flow is considered to be evenly distributed within the dies, and the solder layer is assumed to be free from defects.
2) Due to the encapsulant surrounding the top of the dies, which has low thermal conductivity, it is generally

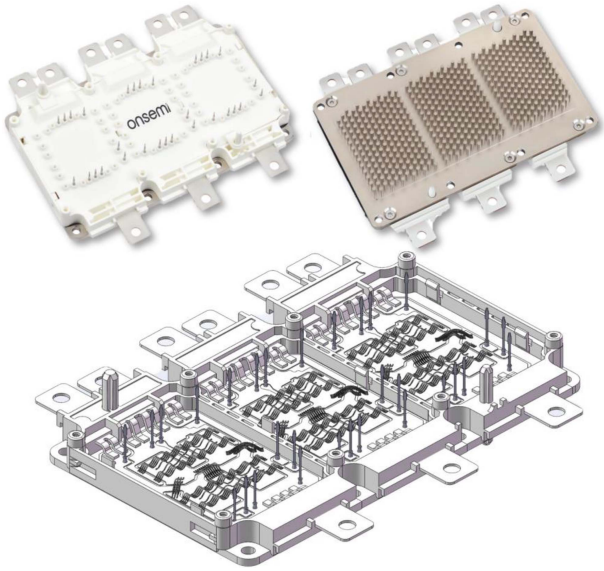

Fig. 3. Onsemi 900-V/620-A power module mechanical structure.

TABLE I
MATERIAL PROPERTIES IN THE ONSEMI 900-V/620-A SIC POWER MODULE

	Material	k[W/(m·K)]	Size[mm]
Dies	SiC	490	6.3 × 4.3 × 0.2
Dies Solder Layer	SAC305	38	6.3 × 4.3 × 0.08
DBC Copper Layer	Cu	380	60 × 40 × 0.3
DBC Ceramic	Si_3N_4	70	60 × 40 × 0.635
Substrate Solder Layer	SAC305	38	60 × 40 × 0.25
Heatsink	Cu	380	152 × 90 × 3
Cold Plate	Al 6061	167	152 × 90 × 18
Coolant	50% Ethylene Glycol	0.406	–

assumed that the dissipated heat flows unidirectionally from top to bottom. Thus, the upper surface of the module is considered as an adiabatic boundary, and radiative heat transfer from the dies is neglected.

3) The aluminum bonding wire within the module is relatively small and is considered to have a negligible impact on heat conduction from the dies.
4) The liquid cooling medium is regarded as an incompressible viscous fluid, with no regard given to the influence of temperature on the thermal properties of the packaging materials.

Fig. 4 shows the structural model and boundary condition settings for the single-sided direct liquid-cooled SiC power module. The cooling fluid's inlet temperature is set at 65 °C, with a flow rate of 10 L/min, and the SiC MOSFET dies' total power loss is specified as 2000 W.

Several parameters have been defined to facilitate the assessment of power module thermal performance metrics, including discretized thermal resistance Z_{thij}, maximum junction-to-fluid thermal resistance R_{thjf}, thermal uniformity index Ψ, and pumping power P.

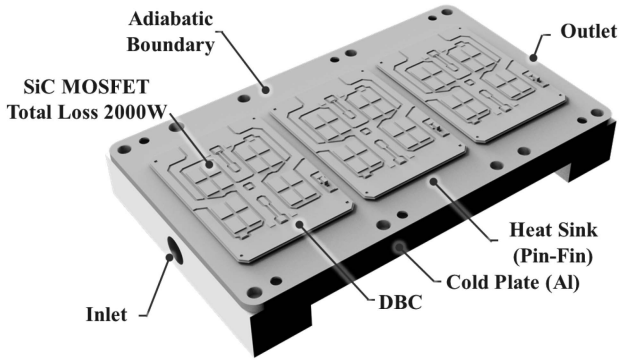

Fig. 4. Power module's simplified model and boundary condition setting.

Thermal resistance can be interpreted as the ratio of the temperature difference across a material to the heat flow passing through it. In power modules, discretized thermal resistance is typically defined at material interfaces, expressed as follows:

$$Z_{thij}(t) = \frac{T_i(t) - T_j(t)}{P_{\text{loss}}(t)} \tag{1}$$

where $T_i(t)$ and $T_j(t)$ represent the temperatures at material interfaces i and j, respectively, and $P_{\text{loss}}(t)$ refers to the total heat loss power.

The steady-state maximum junction-to-fluid thermal resistance of the power module is defined as follows:

$$R_{thjf} = \frac{T_{j\max} - T_{\text{in}}}{P_{\text{loss}}} \tag{2}$$

where $T_{j\max}$ represents the maximum junction temperature of the dies within the module, while T_{in} denotes the inlet fluid temperature. Junction-to-fluid thermal resistance is a critical parameter for evaluating the liquid cooling performance of power modules. Under identical loss conditions, a higher junction-to-fluid thermal resistance leads to an increased junction temperature, substantially affecting the module's operational reliability.

The thermal uniformity index is defined as follows:

$$\Psi = \frac{T_{j\max} - T_{j\min}}{T_{j\max} - T_{\text{in}}} \times 100\% \tag{3}$$

where $T_{j\min}$ represents the maximum junction temperature of the dies within the module. It can quantify the maximum temperature difference between power dies within a module.

In addition, the fluid pressure drop serves as a critical metric for assessing the liquid cooling performance of power modules. When the inlet flow rate remains constant, the fluid pressure drop significantly influences the pumping power of the liquid cooling system

$$P = Q \cdot \Delta p \tag{4}$$

where Q is the inlet flow rate, which is constant in this article, set at 10 L/min. Therefore, the value of P is dependent on the inlet pressure drop Δp.

Fig. 5 shows the simulation results. The internal temperature distribution of the SiC power module under direct cooling with a 65 °C ethylene glycol shows that the maximum junction temperature of the SiC dies is 120.2 °C, accompanied by a maximum

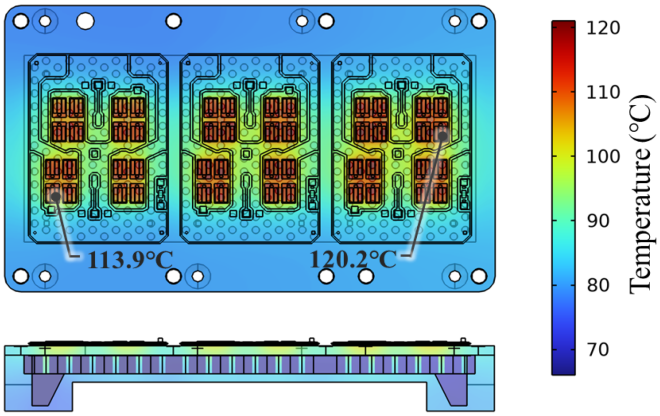

Fig. 5. Simulation results of the Onsemi 900-V/620-A SiC power module.

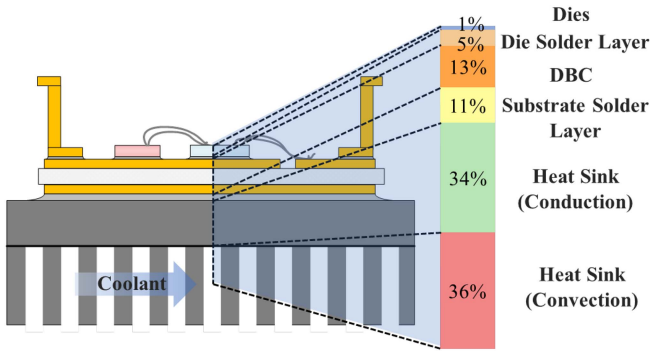

Fig. 6. Thermal resistance distribution in the SiC power module.

temperature difference of 6.3 °C, resulting in a thermal uniformity index as high as 12%. The uneven temperature distribution is mainly due to the use of a series water-cooling layout in the module. During fluid flow, the disturbance created by the pin-fin structure reduces fluid velocity, impacting heat transfer efficiency. This leads to an accumulation of dissipated heat and a gradual increase in fluid temperature, creating a natural temperature gradient. As a result, the junction temperatures of the SiC die near the cooling plate inlet are generally lower than those at the outlet. This uneven temperature distribution may have a negative impact on the long-term reliability of the SiC power module.

Furthermore, the thermal resistance distribution is shown in Fig. 6 by applying (1) to calculate the steady-state thermal resistance of different material layers within the module. It can be observed that the thermal resistance from the top surface of the baseplate to the cooling fluid accounts for as much as 70%, indicating that this pathway is the primary obstacle to efficient heat transfer and emphasizing its significance in thermal optimization design. One effective method for reducing the maximum junction-to-fluid thermal resistance of the direct liquid-cooled SiC power module is to utilize baseplate materials with higher thermal conductivity. This helps to enhance heat transfer efficiency and minimize heat accumulation in the baseplate. Another approach is to design a more efficient liquid cooling structure to increase heat transfer efficiency, which can

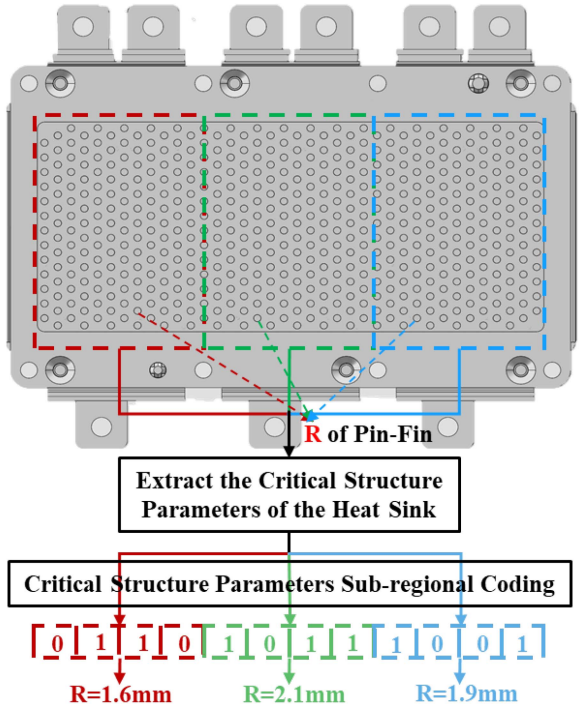

Fig. 7. Heat sink parameterization and subregional coding.

further reduce the convective thermal resistance of the baseplate. This study primarily focuses on designing a more efficient liquid cooling structure for SiC power modules.

B. Design Methodology

In [28] and [29], genetic algorithms have been applied to optimize the cooling structures of Si and SiC power modules, enhancing their thermal performance. In these studies, researchers often partition the heat sink into different regions and suggest multiple structures. The encoding of chromosomes regulates the implementation of diverse structures in different areas, ultimately enhancing the thermal efficiency of the power modules. Although this approach results in heat sinks capable of reducing the maximum thermal resistance, the overall structure still heavily relies on the initially proposed designs, leading to significant human intervention. Furthermore, these studies have not considered optimizing thermal uniformity within the power modules.

Based on the aforementioned analysis, we propose the following optimization method.

1) The heat sink of the power module is divided into three sections, with each half-bridge serving as a unit. This design allows for independent adjustment of the heat sink structures beneath each half-bridge, facilitating different junction-to-fluid thermal resistances for each half-bridge and improving temperature uniformity.
   Before beginning the optimization process, key structural parameters of the heat sink are identified, such as the pillar radius and the spacing between the pillars in both horizontal and vertical directions, as illustrated in Fig. 7. For example, the pillar radius ranges from 1 to 2.5 mm with

a step size of 0.1 mm, resulting in 16 possible pillar radii. To represent these 16 options using binary numbers, a 4-bit binary code is required, where (0, 0, 0, 0) corresponds to a pillar radius of 1 mm and (1, 1, 1, 1) corresponds to 2.5 mm.

This encoding method can also be applied to other structural parameters of the heat sink. As a result, we can use a genetic algorithm for multiobjective optimization to find the optimal set of heat sink parameters that strike a balance between thermal resistance, pressure drop, and thermal uniformity.

2) The NSGA-II is used to encode the critical parameters of the cooling structure for each half-bridge unit in a chromosome, focusing on optimizing the maximum thermal resistance, thermal uniformity, and pressure drop of the power module as multiobjective optimization objectives. To improve the efficiency and performance of the genetic algorithm, the NSGA-II has undergone the following enhancements.
   a) *Fast nondominated sorting:* The integration of fast nondominated sorting has significantly decreased computational complexity, enabling the efficient identification of Pareto-optimal solutions, even within extensive search spaces.
   b) *Crowding distance concept:* Incorporating the crowding distance concept significantly enhances the genetic algorithm's global search capability.
   By assessing the distribution of individuals in the objective space, priority is given to individuals situated in crowded regions, thereby upholding the diversity of solutions.
   c) *Elitism strategy:* This strategy helps retain the high-quality individuals from parent population by combining the parent population with its offspring for competitive selection. It ensures that optimal solutions are carried forward into subsequent iterations, improving overall optimization outcomes.

Through these enhancements, the NSGA-II is capable of more effectively exploring the design space of cooling structures and identifying superior cooling solutions. Consequently, this leads to an improvement in the thermal management performance of power modules.

The process delineated in Fig. 8 includes using COMSOL to parameterize the cooling structure and execute multiphysics simulations. Concurrently, the NSGA-II is implemented in MATLAB. These two platforms interface through COMSOL Multiphysics with MATLAB, facilitating the comprehensive realization of the optimization process.

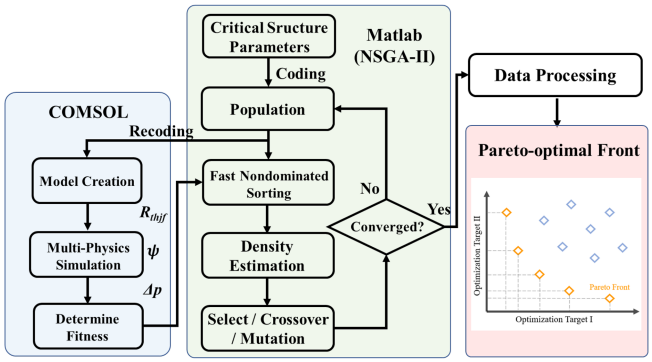

Fig. 8. Heat sink optimization method based on the NSGA-II and FEA.

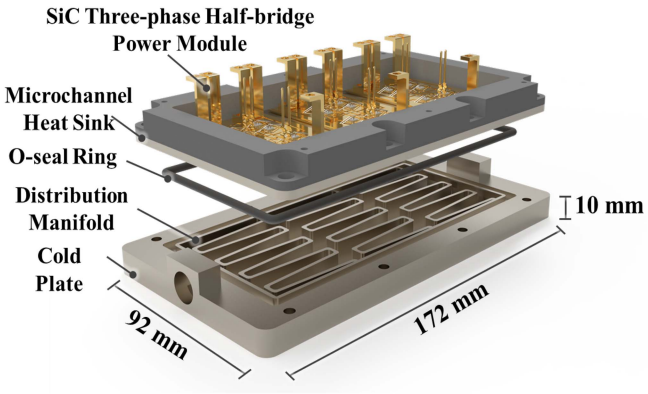

Fig. 9. Configuration of the power module integrated with the MMC heat sink.

III. Optimization of the MMC Heat Sink

A. Design of the SiC Power Module With the MMC Heat Sink

In order to optimize the thermal performance of the MMC direct liquid cooling heat sink, this section designs a direct liquid-cooled SiC three-phase half-bridge power module with an MMC heat sink based on the size of Onsemi commercial SiC power modules. Its mechanical structure is shown in Fig. 9. This power module consists of three half-bridge direct bonded copper (DBC) substrates fixed to a copper baseplate integrated with an MMC heat sink using welding. Each phase leg uses four 1.2-kV SiC MOSFET dies (Rohm S4108) in a parallel configuration, with a rated current of 124 A and no reverse parallel schottky barrier diode (SBD) dies. The SiC three-phase half-bridge power module is bolted to an aluminum alloy cold plate using a sealing gasket and connected to an external circulating liquid cooling system. Table II provides detailed material parameters for the power module, cold plate, and cooling fluid.

TABLE II
Material Properties in the SiC Power Module

	Material	k [W/(m·K)]	Size [mm]
Dies	SiC	490	3.06 × 2.45 × 0.38
Dies Solder Layer	SAC305	38	3.06 × 2.45 × 0.15
DBC Copper Layer	Cu	380	60 × 40 × 0.3
DBC Ceramic Substrate	AlN	160	60 × 40 × 0.63
Solder Layer	SAC305	38	60 × 40 × 0.25
Microchannel	Cu	380	130 × 0.6 × 1
Cold Plate	Al 6061	167	152 × 90 × 10
Coolant	Deionized Water	0.609	–

Fig. 10 shows the cooling fluid flow path within the MMC liquid cooling structure. The cold plate is equipped with a

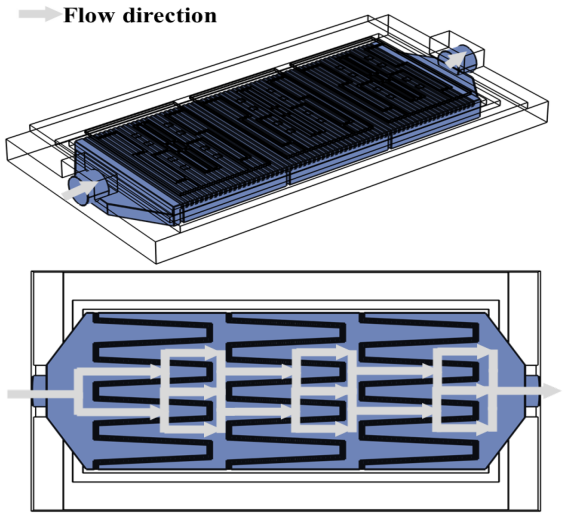

Fig. 10. Coolant flow path in the MMC.

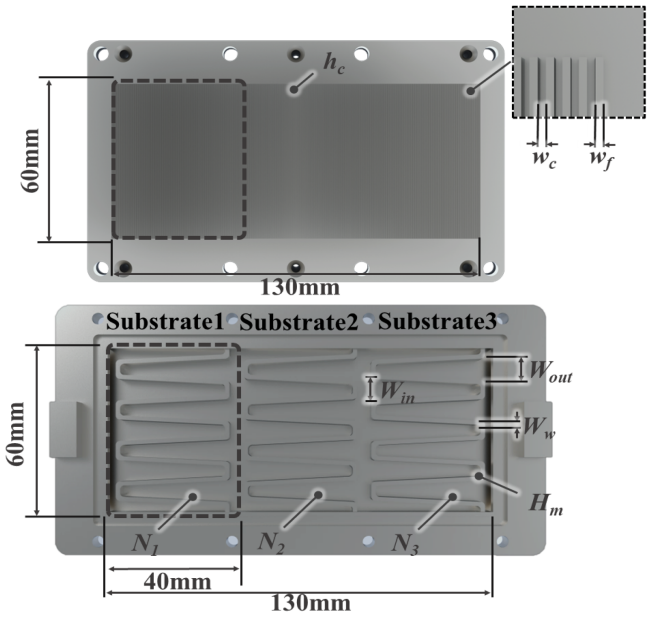

Fig. 11. Parametric modeling of the MMC heat sink.

series flow channel arrangement to ensure a sufficient amount of cooling medium flows beneath the heat source to minimize the thermal resistance between the SiC power module and the cooling fluid. After entering the cold plate, the cooling fluid first passes through a conical buffering layer at the inlet, which promotes a more uniform flow distribution and reduces local overheating caused by uneven flow distribution. Subsequently, the fluid sequentially flows through the diverging manifold directly below the three half-bridge DBC substrates, exchanging heat with the corresponding microchannel baseplate, and finally converges at the outlet's conical buffering layer before exiting the cold plate. This series flow design further enhances the disturbance of the fluid, helping to disrupt the stable development of the thermal boundary layer, thereby reducing the accumulation effect of dissipated heat in any single region of the flow channel and maximizing the liquid cooling heat transfer efficiency.

B. Parametric Modeling of the MMC Heat Sink

The critical parameters of the MMC liquid cooling structure mainly include the inlet channel width W_{in}, outlet channel width W_{out}, channel height H_m, channel wall thickness W_w, number of channels N, as well as the fin thickness w_f, flow channel width w_c, and flow channel depth h_c in the microchannel structure, as shown in Fig. 11. Studies have shown that the effects of these structural parameters on overall thermal resistance, fluid pressure drop, and temperature distribution uniformity are not monotonically increasing or decreasing. In order to attain the optimal parameter combination, it is essential to strike a balance between high heat transfer efficiency and low fluid pressure drop while mitigating temperature distribution nonuniformity.

The core objective of optimizing the MMC heat sink is to optimize thermal performance within the constraints of a specified volume or weight limit. Therefore, during the optimization process, the total height of the MMC liquid cooling structure must remain constant, meaning that the sum of channel height H_m and flow channel depth h_c is unchanged. Furthermore, in order to maximize the benefits of microchannel liquid cooling technology and address constraints related to minimum processing dimensions and potential flow channel blockage risks, this study restricts the values of fin thickness w_f and flow channel width w_c to be between 0.2 and 0.6 mm and specifies that the fin thickness equals the flow channel width to reduce the number of optimization decision variables. Each structural parameter of the bifurcated manifold is designed separately, where the bifurcated manifold adopts a conical structure with a width ratio of 2 at the inlet and the outlet. By optimizing the number of parallel channels in the manifold region, we can indirectly adjust the flow path of the cooling fluid and the impact of the jet on the structure. This helps to reduce the nonuniform distribution of temperature among the three half-bridge DBC substrates of the SiC power module.

In conclusion, the optimization decision variables for the SiC power module MMC heat sink have been refined to five. The multiobjective optimization problem can be expressed as follows:

$$\begin{cases} \text{Min}: R_{thjf}, \Delta p, \psi \\ \text{s.t.} \;\; 0.2\,\text{mm} \le w_f = w_c \le 0.6\ \text{mm} \\ \qquad 0.5\,\text{mm} \le h_c \le 2.5\ \text{mm} \\ \qquad H_m + h_c = 8\,\text{mm} \\ \qquad W_{\text{in}} = W_{\text{out}} \\ \qquad W_w = 1.6\,\text{mm} \\ \qquad 2 \le N_i \le 6, i = 1, 2, 3. \end{cases} \tag{5}$$

C. Optimal Solution Set and Simulation Validation for the MMC Heat Sink

Following the optimization process outlined in Section II, we conducted an optimization of the self-designed power module. Given that the thermal–hydraulic collaborative multiobjective

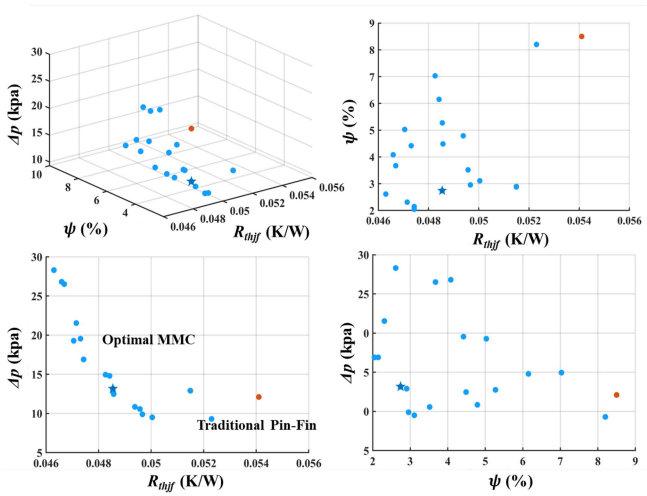

Fig. 12. Pareto-optimal front of R_{thjf}, Ψ, and Δp.

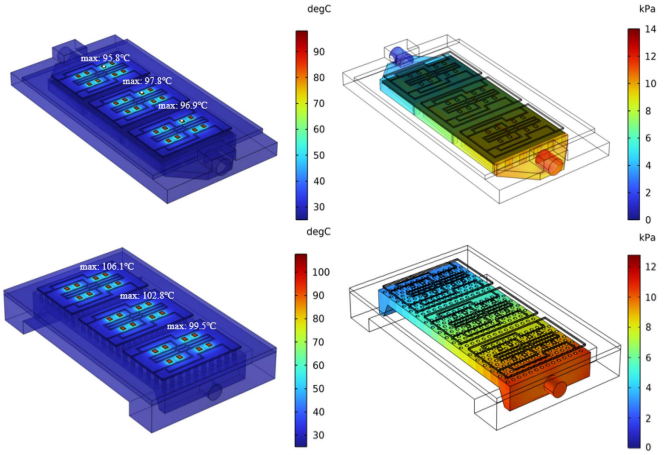

Fig. 13. Simulation results of the power module with the optimized MMC heat sink (up) and the traditional pin-fin heat sink (bottom).

TABLE III
PARAMETERS OF THE OPTIMAL MMC HEAT SINK

w_f (mm)	w_c (mm)	h_c (mm)	H_m (mm)	N_1	N_2	N_3
0.2	0.2	1.5	6.5	5	4	3

TABLE IV
PARAMETERS OF THE TRADITIONAL PIN-FIN HEAT SINK

D_h (mm)	D_v (mm)	R (mm)
4.2	3.6	1.1

optimization involves the integration of multiple software simulations and that each evaluation necessitates solving complex turbulent heat transfer equations, the computational load during the optimization process is substantial. Therefore, we set the population size of the NSGA-II optimization algorithm to 30, with a maximum iteration limit of 20, and specified crossover and mutation probabilities of 0.8 and 0.1, respectively. Upon running the simulation optimization program, we obtained the Pareto-optimal solution set, as illustrated in Fig. 12. The blue points on the Pareto front represent the parameters of the MMC liquid cooling structure that dominate in terms of thermal–hydraulic resistance, fluid pressure drop, and thermal uniformity. The blue pentagram indicates the optimal MMC liquid cooling structure with superior performance across all metrics, while the orange points correspond to the parameters of the traditional pin-fin liquid cooling structure, which underperforms relative to the Pareto-optimal solutions of the MMC liquid cooling structure.

The structural parameters for the optimal MMC liquid cooling structure and the traditional pin-fin liquid cooling structure are listed in the accompanying Tables III and IV, where D_h is the longitudinal spacing of the pins, D_v is the vertical spacing of the pins, and R is the radius of the pins.

We conduct thermal–hydraulic simulations under identical boundary conditions for SiC power modules integrating both the optimized MMC heat sink and the traditional pin-fin heat sink. The simulation results are shown in Fig. 13. Under power loss of 1500 W, the former exhibits a maximum junction temperature of 97.8 °C with a maximum temperature difference of 2.0 °C between the half-bridges, and the latter exhibits a maximum junction temperature of 106.1 °C, with a maximum temperature difference of 6.6 °C between the half-bridges.

The former exhibits a 10.4% reduction in junction-to-fluid thermal resistance compared to the latter. In addition, the thermal nonuniformity decreased by 66.2% compared to the power module with a traditional pin-fin heat sink, indicating a significant improvement in thermal performance. It is important to note that the pressure drop in the optimized MMC heat sink increased by 1.2 kPa compared to the traditional pin-fin heat sink. However, this slight increase does not have a significant impact on the overall liquid cooling system performance.

IV. EXPERIMENTAL VERIFICATION

A. Fabrication of the Power Module

Based on the direct liquid cooling SiC three-phase half-bridge power module mentioned in Section III, the entire die soldering and module assembly process is completed in the laboratory, as shown in Fig. 14. Prior to commencement, the SiC MOSFET dies are extracted from the wafer, and the DBC substrate with etched circuit patterns, along with graphite fixtures for position stabilization, is prepared. The individual half-bridge DBC substrate is then placed in the graphite fixture, and precut solder pads are added, along with the SiC MOSFET dies and power terminals, to undergo the first reflow soldering process. Subsequently, wire bonding technology is utilized to establish connections between the SiC MOSFET dies and the upper layer copper of the DBC substrate, ensuring a complete circuit connection. Finally, the graphite fixture is used to secure the position again, and a secondary reflow soldering process is carried out to attach the three half-bridge DBC substrates to the corresponding heat sink base, while the housing is secured to the heat sink with bolts and metal adhesive. The entire processing flow of the SiC power module aligns closely with conventional module packaging techniques, and the optimized MMC heat sink does not incur additional

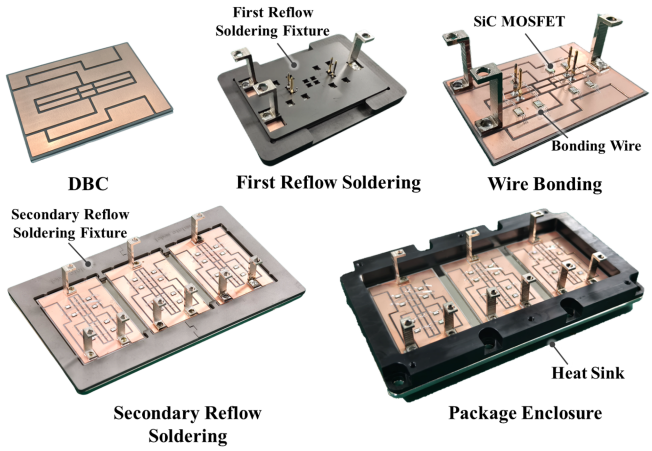

Fig. 14. Fabrication of the power module.

TABLE V
ESSENTIAL COMPONENTS AND MATERIAL PROPERTIES OF THIS POWER MODULE

	Material	Description
Dies	SiC	RohmS4108,1200V/31 A
Bonding Wire	Al	Diameter (10 mil)
DBC	AlN	Copper (0.3 mm) AlN (0.63 mm)
Solder	SAC305	———
Power Terminal	Cu	Thickness (2 mm) Nickel Plating
Heatsink	Cu	CNC, Nickel Plating
Cold Plate	Al6061	CNC, Surface Oxidation
Enclosure	Polyetherether ketone	Temperature Resistance (260 °C)
Fixture	Plumbago	Thickness (10 mm)

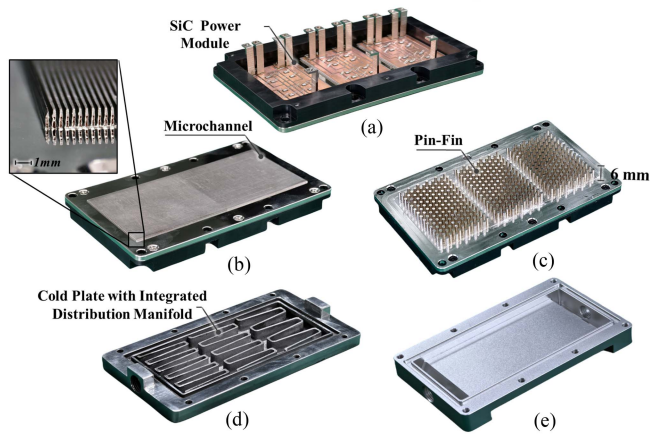

Fig. 15. Power module with different heat sink. (a) SiC power module. (b) Optimized MMC heat sink. (c) Traditional pin-fin heat sink. (d) Cold plate for the MMC heat sink. (e) Cold plate for the traditional pin-fin heat sink.

equipment or process expenses. The essential components and material properties of this power module are summarized in Table V.

Fig. 15 shows power modules integrated with the traditional pin-fin heat sink and the optimized MMC heat sink, along with their cold plates.

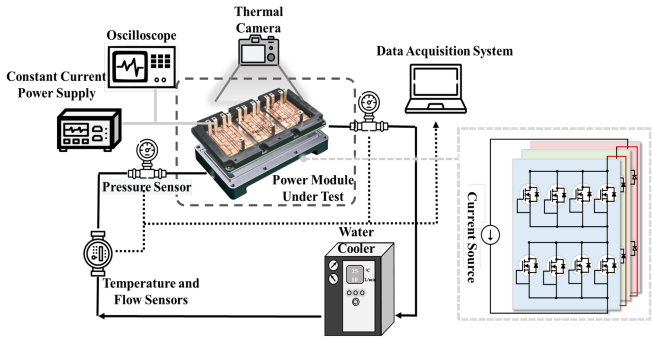

Fig. 16. Schematic of the thermal testing platform.

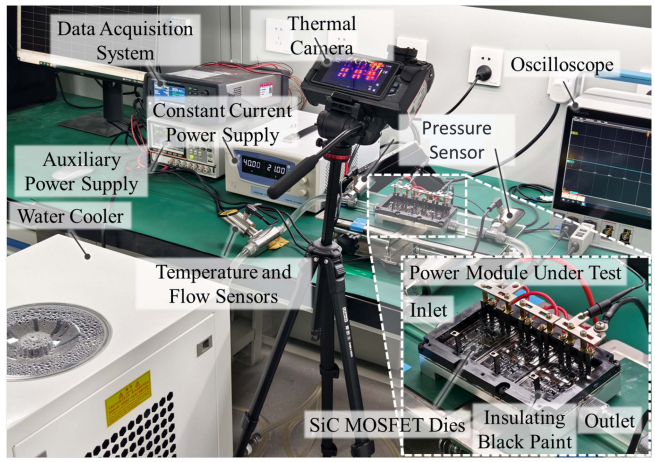

Fig. 17. Experimental setup for the SiC power module thermal test.

B. Experimental Setup

To ensure the accuracy and fairness of the test results, avoid influences from external factors, such as heat source distribution, thermal radiation, power loss, and measurement systems. A dedicated testing platform for the direct liquid cooling performance of the SiC power module is established. Its schematic is shown in Fig. 16.

The specific experimental setup for testing the liquid cooling performance is shown in Fig. 17. Deionized water is used as the coolant, and the entire liquid cooling system is powered by an external recirculating water cooler, which maintained the coolant temperature at the inlet of the SiC power module's cold plate at a constant 25 °C. The flow rate is precisely adjusted using control valves. Flow and temperature sensors (with an accuracy of 0.2%) are positioned at the outlet of the recirculating water cooler to monitor the actual flow rate and temperature of the inlet fluid. In addition, precision pressure sensors (range 600 kPa and accuracy 0.2%) are installed near both the inlet and outlet sides of the SiC power module cold plate to measure the actual pressure at these points.

A constant current power supply (0–30 V and 0–100 A) is utilized to power the three-phase half-bridge SiC power module. To simplify the experiment, the three half-bridge DBC substrates are connected in series to ensure consistent current flow, and the

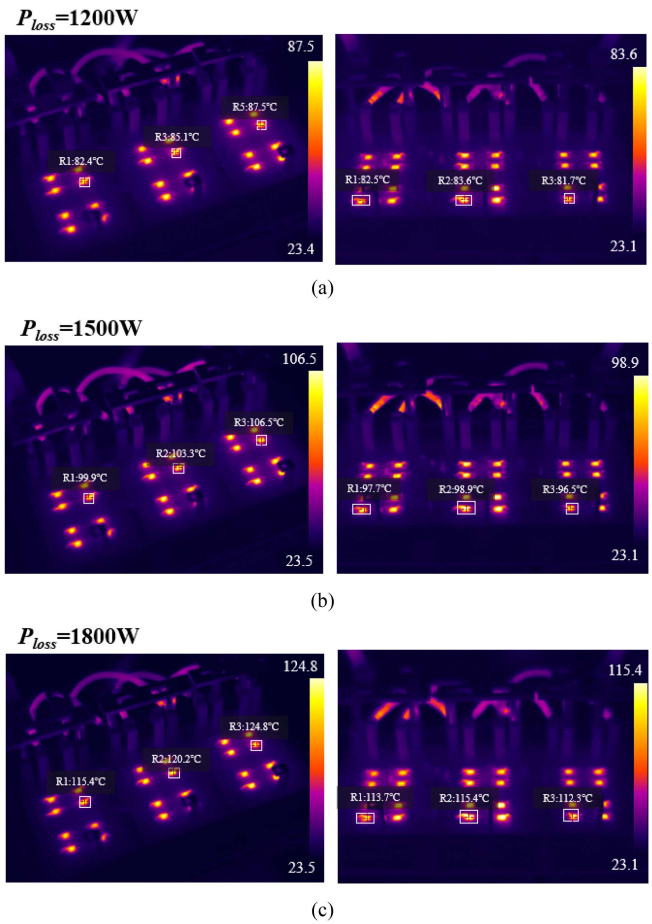

Fig. 18. Temperature distribution of the power module with the traditional pin-fin heat sink (left) and the optimized MMC heat sink (right) in the infrared thermal imaging camera under (a) power loss of 1200 W, (b) power loss of 1500 W, and (c) power loss of 1800 W.

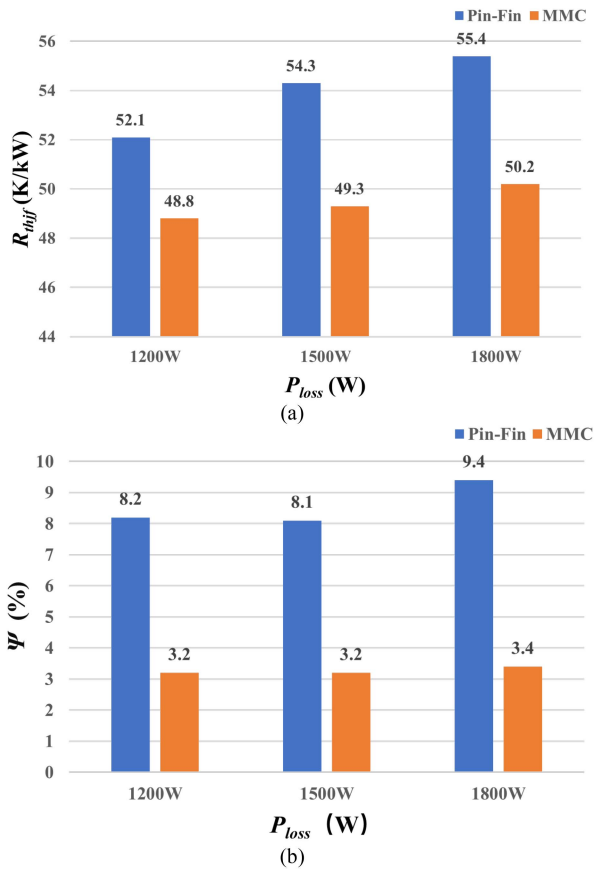

Fig. 19. Comparison of (a) R_{thjf} and (b) Ψ under different power loss.

gate and source terminals of the SiC MOSFET dies are shorted, allowing for reverse current flow through the body diodes, utilizing body diode loss to act as a heat source.

To facilitate precise temperature measurement of the SiC power module, a uniform coating of black insulating paint with an emissivity of approximately 0.96 is applied to the upper surface of the DBC substrate. Subsequently, an infrared thermal imaging camera (Guide PS610) is utilized for temperature assessment.

During the experiment, the flow rate, temperature, and inlet and outlet pressure signals of the liquid cooling system are recorded using a data acquisition system (Keysight DAQ970A) and monitored in real time with corresponding software. The actual input voltage, current, and power loss of the SiC power module are measured using an oscilloscope.

C. Experimental Results

The coolant flow rate is maintained at 10 L/min, and the steady-state temperature distribution of the SiC power module under different power loss conditions is shown in Fig. 18. As the power loss of the module increases, the maximum junction temperature of the SiC die rises correspondingly, and temperature difference between the three half-bridge DBC substrates also increases.

Compared with the traditional pin-fin heat sink, the optimized MMC heat sink demonstrated a notable reduction in both the maximum junction temperature of the dies and the temperature difference between the half-bridge substrates.

Fig. 19 presents R_{thjf} and Ψ of the power module using the traditional pin-fin heat sink and the optimized MMC heat sink under different power loss. It can be observed that R_{thjf} and Ψ of the power module integrated with the optimized MMC heat sink are lower than the power module integrated with the traditional pin-fin heat sink.

Under the power loss of 1500 W, the maximum junction temperature of the power module integrating traditional pin-fin heat sink reached 106.5 °C. The maximum temperature difference is 6.6 °C, resulting in a maximum junction-to-fluid thermal resistance of 54.3 K/kW and a thermal nonuniformity of 8.1%. In contrast, the power module integrating the optimized MMC heat sink exhibited a maximum junction temperature of 98.9 °C and a maximum temperature difference of 2.4 °C, with a maximum junction-to-fluid thermal resistance of 49.3 K/W and a thermal nonuniformity of only 3.6%. This indicates that the optimized MMC heat sink achieved a reduction of 9.2% in maximum junction-to-fluid thermal resistance and a 55.6%

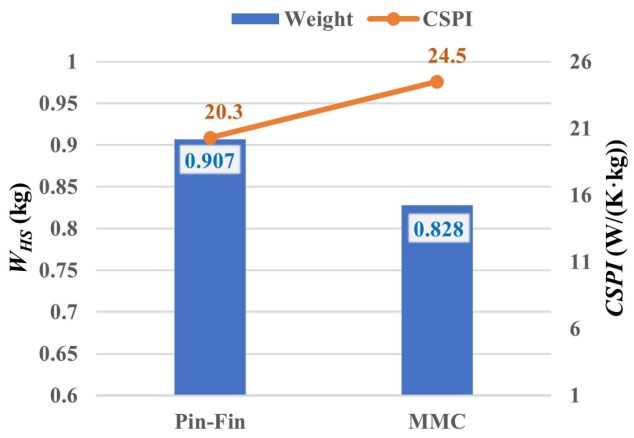

Fig. 20. Comparison of CSPI of the SiC power module integrating the traditional pin-fin heat sink and the optimized MMC heat sink.

decrease in thermal nonuniformity, which is conducive to the long-term reliability of the SiC power modules.

However, it is worth noting that the optimized MMC heat sink exhibited an increase in fluid pressure drop across the cold plate, rising by 1.4 kPa compared with the traditional pin-fin heat sink. This increase can be attributed to two main factors.

1) The flow mode design introduced jet impact effects, increasing fluid disturbance.
2) To reduce overall weight, the cold plate is designed with a more compact structure, decreasing its height from 18 to 10 mm. This modification has led to an increase in pressure drop due to the narrower flow channels.

Nonetheless, this pressure drop increase is unlikely to affect conventional liquid cooling systems significantly.

Overall, excluding the dies' differences, processing and assembly errors, and measurement errors, the experiment and simulation are basically consistent with each other.

In addition, to quantify the power density metrics of the power module, the heat dissipation performance indicator related to weight, known as cooling system performance index (CSPI) [30], can be utilized. The specific definition is as follows:

$$\text{CSPI} = \frac{1}{R_{thjf} \times W_{HS}} \tag{6}$$

where W_{HS} is the weight of power module with the cold plate.

Fig. 20 shows W_{HS} and CSPI metrics of two different direct liquid-cooled SiC power module structures under power loss of 1500 W. Compared to the power module integrating the traditional pin-fin heat sink, the power module integrating the MMC heat sink exhibited a total weight reduction of 8.7%, while the CSPI improved by 20.7%. This demonstrates that the optimized MMC heat sink significantly enhances the power density of the SiC power module, making it highly suitable for lightweight and high-heat-flux applications.

V. Conclusion

In this article, a new MMC heat sink is proposed as a potential solution to the thermal management challenges linked to high-heat-flux density and poor thermal uniformity in SiC power modules. An automated multiobjective optimization method based on the NSGA-II and FEA is proposed to optimize the MMC heat sink. Experimental results verify that the power module integrating the new MMC heat sink can achieve a 9.2% reduction in maximum junction-to-coolant thermal resistance, a 55.6% enhancement in thermal uniformity, and an 8.7% decrease in total weight when subjected to a power loss of 1500 W, compared to the power module integrating the traditional pin-fin heat sink.

References

[1] S. Otake et al., "Heatsink design using spiral-fins considering additive manufacturing," in *Proc. Int. Conf. Electron. Packag.*, 2019, pp. 46–51.
[2] K. Rajashekara, "Present status and future trends in electric vehicle propulsion technologies," *IEEE J Emerg. Sel Top. Power Electron.*, vol. 1, no. 1, pp. 3–10, Mar. 2013.
[3] C. Qian et al., "Investigation of reverse recovery phenomenon for SiC MOSFETs in high-temperature applications," *IEEE Trans. Power Electron.*, vol. 38, no. 11, pp. 14375–14387, Nov. 2023.
[4] Y. Chen, B. Li, X. Wang, Y. Yan, Y. Wang, and F. Qi, "Investigation of heat transfer and thermal stresses of new thermal management system integrated with vapour chamber for IGBT power module," *Thermal Sci. Eng. Prog.*, vol. 10, pp. 73–81, May 2019.
[5] Y. Wu, Z. Wang, X. Yan, G. Xin, X. Shi, and Y. Kang, "Conduction thermal runaway of SiC MOSFET under natural convection heat dissipation," in *Proc. IEEE 2nd Int. Power Electron. Appl. Symp.*, 2023, pp. 125–129.
[6] H. Wang, M. Liserre, and F. Blaabjerg, "Toward reliable power electronics: Challenges design tools and opportunities," *IEEE Ind. Electron. Mag.*, vol. 7, no. 2, pp. 17–26, Jun. 2013.
[7] U.S. Department of Energy. US DRIVE Electrical and Electronics Roadmap [EB/OL]. Oct. 2017. Accessed: Apr. 17, 2024. [Online]. Available: https://www.energy.gov/eere/vehicles/articles/us-drive-electrical-and-electronics-technical-team-roadmap
[8] B. S. Passmore and A. B. Lostetter, "A review of SiC power module packaging technologies: Attaches interconnections and advanced heat transfer," in *Proc. IEEE Int. Workshop Integr. Power Packag.*, Apr. 2017, pp. 1–5.
[9] I. Aranzabal, I. M. de Alegría, N. Delmonte, P. Cova, and I. Kortabarria, "Comparison of the heat transfer capabilities of conventional single- and two-phase cooling systems for an electric vehicle IGBT power module," *IEEE Trans. Power Electron.*, vol. 34, no. 5, pp. 4185–4194, May 2019.
[10] C.-W. Chang, X. Zhao, R. Phukan, D. Dong, R. Burgos, and A. Plat, "Weight-minimizing optimization of microchannel cold plate for SiC-based power inverters in more-electric aircraft," in *Proc. IEEE Energy Convers. Congr. Expo.*, Detroit, MI, USA, 2022, pp. 1–8.
[11] M. S. Zaman et al., "Multiphysics optimization of thermal management designs for power electronics employing impingement cooling and stereolithographic printing," *IEEE Trans. Power Electron.*, vol. 36, no. 11, pp. 12769–12780, Nov. 2021.
[12] Y. Chen et al., "Direct phase-change cooling of vapor chamber integrated with IGBT power electronic module for automotive application," *IEEE Trans. Power Electron.*, vol. 36, no. 5, pp. 5736–5747, May 2021.
[13] L. Wang et al., "Forced fluorinated liquid cooling for medium voltage SiC power modules: Concurrently addressing electrical and thermal challenges," *IEEE Trans. Power Electron.*, vol. 39, no. 12, pp. 15622–15634, Dec. 2024.
[14] X. Chen, X. Xu, M. Li, Y. Li, and H. Ling, "Multi-objective topology optimization design of silicon carbide metal oxide semiconductor field effect transistors power module liquid-cooled heatsink for electric vehicles," *Appl. Thermal Eng.*, vol. 254, 2024, Art. no. 123861.
[15] F. Han, H. Guo, and X. Ding, "Design and optimization of a liquid cooled heat sink for a motor inverter in electric vehicles," *Appl. Energy*, vol. 291, Jun. 2021, Art. no. 116819.
[16] Z. Wang, M. Chinthavali, S. L. Campbell, T. Wu, and B. Ozpineci, "A 50-kW air-cooled SiC inverter with 3-D printing enabled power module packaging structure and genetic algorithm optimized heatsinks," *IEEE Trans. Power Electron.*, vol. 55, no. 6, pp. 6256–6265, Nov./Dec. 2019.

[17] K. W. Jung et al., "Microchannel cooling strategies for high heat flux (1 kW/cm^2) power electronic applications," in *Proc. 16th IEEE Intersoc. Conf. Thermal Thermomech. Phenomena Electron. Syst.*, May 2017, pp. 98–104.
[18] R. van Erp, G. Kampitsis, and E. Matioli, "Efficient microchannel cooling of multiple power devices with compact flow distribution for high power-density converters," *IEEE Trans. Power Electron.*, vol. 35, no. 7, pp. 7235–7245, Jul. 2020.
[19] R. V. Erp, G. Kampitsis, and E. Matioli, "A manifold microchannel heat sink for ultra-high power density liquid-cooled converters," in *Proc. IEEE Appl. Power Electron. Conf. Expo.*, 2019, pp. 1383–1389.
[20] E. Kermani, S. Dessiatoun, A. Shooshtari, and M. Ohadi, "Experimental investigation of heat transfer performance of a manifold microchannel heat sink for cooling of concentrated solar cells," in *Proc. 59th Electron. Compon. Technol. Conf.*, May 2009, pp. 453–459.
[21] I. L. Collins, J. A. Weibel, L. Pan, and S. V. Garimella, "Evaluation of additively manufactured microchannel heat sinks," *IEEE Trans. Compon., Packag. Manuf. Technol.*, vol. 9, no. 3, pp. 446–457, Mar. 2019.
[22] M. A. Arie, A. H. Shooshtari, S. V. Dessiatoun, E. Al-Hajri, and M. M. Ohadi, "Numerical modeling and thermal optimization of a single-phase flow manifold-microchannel plate heat exchanger," *Int. J. Heat Weight Transfer*, vol. 81, pp. 478–489, 2015.
[23] N. Gilmore, V. Timchenko, and C. Menictas, "Manifold microchannel heat sink topology optimisation," *Int. J. Heat Weight Transfer*, vol. 170, 2021, Art. no. 121025.
[24] D. Kong et al., "A holistic approach to thermal-hydraulic design of 3D manifold microchannel heat sinks for energy-efficient cooling," *Case Study Thermal Eng.*, vol. 28, 2021, Art. no. 101583.
[25] R. Whitt, D. Huitink, A. Emon, A. Deshpande, and F. Luo, "Thermal and electrical performance in high-voltage power modules with nonmetallic additively manufactured impingement coolers," *IEEE Trans. Power Electron.*, vol. 36, no. 3, pp. 3192–3199, Mar. 2021.
[26] X. Perpinà, O. Garonne, J. P. Rochet, P. Jalby, M. Mermet-Guyennet, and J. Rebollo, "Experimental analysis of temperature distribution within traction IGBT modules," in *Proc. 12th Eur. Conf. Power Electron. Appl.*, 2007, pp. 1–10.
[27] K. Deb, A. Pratap, S. Agarwal, and T. Meyarivan, "A fast and elitist multiobjective genetic algorithm: NSGA-II," *IEEE Trans. Evol. Comput.*, vol. 6, no. 2, pp. 182–197, Apr. 2002.
[28] T. Wu, Z. Wang, B. Ozpineci, M. Chinthavali, and S. Campbell, "Automated heatsink optimization for air-cooled power semiconductor modules," *IEEE Trans. Power Electron.*, vol. 34, no. 6, pp. 5027–5031, Jun. 2019.
[29] Y. Liao, Z. Wang, Y. Yang, G. Xin, and X. Shi, "Microchannel cold plate with GA optimized manifold for enhanced local cooling of SiC power modules," in *Proc. IEEE Energy Convers. Congr. Expo.*, Nashville, TN, USA, 2023, pp. 6034–6038.
[30] K. Yamaguchi, K. Katsura, T. Yamada, and Y. Sato, "High power density SiC-based inverter with a power density of 70 kW/liter or 50 kW/kg," *IEEJ J. Ind. Appl.*, vol. 8, no. 4, pp. 694–703, 2019.

Chunyang Man (Student Member, IEEE) was born in Inner Mongolia, China. He received the B.S. degree in ocean engineering in 2023 from the Huazhong University of Science and Technology, Wuhan, China, where he is currently working toward the Ph.D. degree in electrical engineering with the School of Electrical and Electronic Engineering.

His research interests include packaging and integration of silicon carbide power semiconductor modules, and advanced thermal management for power devices.

Zhiqiang (Jack) Wang (Senior Member, IEEE) received the B.S. degree from Hunan University, Changsha, China, in 2007, and the M.S. degree from Zhejiang University, Hangzhou, China, in 2010, both in electrical engineering, and the Ph.D. degree in electrical engineering from the University of Tennessee, Knoxville, TN, USA, in 2015.

He was with the Power Electronics and Electric Machinery Research Center, Oak Ridge National Laboratory, Oak Ridge, TN, as a Postmaster Research Associate from 2014 to 2015, a full-time R&D Associate Staff Member from 2015 to 2018, and an R&D Staff Member in 2019. Since 2018, he has been an Adjunct Professor with the University of Tennessee. He is currently a Full Professor with the Huazhong University of Science and Technology, Wuhan, China. He has authored and coauthored more than 80 publications in international conferences and journals. His research interests include packaging and integration of wide-bandgap power semiconductor devices, and their applications to high-temperature, high-frequency, and high-density power electronic systems.

Dr. Wang was the recipient of more than ten awards from the Oak Ridge National Laboratory and IEEE. He was the Technical Program Chair for 2021 IEEE Workshop on Wide Bandgap Power Devices and Applications in Asia. He is the Transaction Paper Review Chair for the Power Electronics Devices and Components Committee of the IEEE Industry Applications Society.

Yu Liao (Student Member, IEEE) was born in Guangdong, China. He received the B.S. and M.S. degrees in electrical engineering from the Huazhong University of Science and Technology, Wuhan, China, in 2021 and 2024, respectively.

His research interests include packaging and integration of silicon carbide power semiconductor modules, and advanced thermal management for power devices.

Xiaojie Shi (Senior Member, IEEE) received the M.S. degree from Zhejiang University, Hangzhou, China, in 2011, and the Ph.D. degree from the University of Tennessee, Knoxville, TN, USA, in 2015, both in electrical engineering.

In 2016, she was a Research Assistant Professor with the Center for Ultra-Wide-Area Resilient Electric Energy Transmission Networks, University of Tennessee. From 2017 to 2019, she was an Engineer/Scientist II with the Electric Power Research Institute, Knoxville, where she was also an Engineer/Scientist III from 2020 to 2021. Since 2019, she has been an Adjunct Professor with the University of Tennessee. She is currently a Full Professor with the Huazhong University of Science and Technology, Wuhan, China. She has authored/coauthored more than 60 publications in international conferences and journals. Her research interests include driving and protection of power semiconductor devices, modeling and control of grid-connected power converters, microgrid design, and operation.

Guoqing Xin (Member, IEEE) received the B.S. degree in chemistry from Shandong University, Jinan, China, in 2009, the M.S. degree in chemical engineering from Sungkyunkwan University, Suwon, South Korea, in 2011, and the Ph.D. degree in mechanical engineering from Rensselaer Polytechnic Institute, Troy, NY, USA, in 2016.

From 2016 to 2017, he was a Postdoctoral Researcher with Rensselaer Polytechnic Institute. From 2017 to 2019, he was a Senior Process Engineer with Global Foundries, Malta, NY. He is currently a Full Professor with the Huazhong University of Science and Technology, Wuhan, China. He has authored and coauthored more than 40 technical papers in journals and conference proceedings. His research interests include wide-bandgap semiconductor devices fabrication, thermal management of power electronics, and high-temperature modules for power electronic applications.

Yonggang Yao (Member, IEEE) received the Ph.D. degree in electrical engineering from the University of Maryland, College Park, MD, USA, in 2018.

He is currently a Professor with the School of Materials Science and Engineering, Huazhong University of Science and Technology, Wuhan, China. He has authored or coauthored more than 100 papers in high-profile journals, such as *Science*, *Nature*, *Nature Nanotechnology*, *Nature Catalysis*, and *Science Advances*, with a total citation of more than 10 000. His research interests include the transient high-temperature synthesis and data-driven material discovery.

Dr. Yao is the recipient of the 2020 "R&D 100 Award," the 2022 Metals Young Investigator Award, the 2022 DAMO Young Academy Fellowship, and MIT TR35 China. He has also been ranked "Highly-Cited Researchers" by Clarivate.

Run Hu (Member, IEEE) received the B.S. and Ph.D. degrees in energy engineering from the Huazhong University of Science and Technology (HUST), Wuhan, China, in 2010 and 2015, respectively.

He was a Visiting Scholar with Purdue University, West Lafayette, IN, USA. He was a Japan Society for the Promotion of Science Postdoctoral Fellow with the University of Tokyo, Tokyo, Japan. He is currently a Full Professor with the School of Energy and Power Engineering, HUST. He has authored more than 100 publications in journals. His main research interests include heat and mass transfer, thermal metamaterials and functional devices, and thermal management of optoelectronic devices.